AGU PUBLICATIONS

Geophysical Research Letters

RESEARCH LETTER
10.1002/2014GL060155

Key Points:
- Sediment transport is reduced in a plant patch
- Morphological response is an increase of bed slope to accommodate sediment flux
- Final bed slope and adjustment time scale depend on a skin friction coefficient

Supporting Information:
- Readme
- Supplementary material
- Supplementary material
- Supplementary material
- Figure S1

Correspondence to:
C. Le Bouteiller,
caroline.le-bouteiller@irstea.fr

Citation:
Le Bouteiller, C., and J. G. Venditti (2014), Vegetation-driven morphodynamic adjustments of a sand bed, *Geophys. Res. Lett.*, *41*, doi:10.1002/2014GL060155.

Received 7 APR 2014
Accepted 12 MAY 2014
Accepted article online 14 MAY 2014

Vegetation-driven morphodynamic adjustments of a sand bed

Caroline Le Bouteiller[1,2] and Jeremy G. Venditti[1]

[1]Department of Geography, Simon Fraser University, Burnaby, British Columbia, Canada, [2]Now at IRSTEA, UR ETNA, Saint-Martin d'Heres, France

Abstract Vegetation is ubiquitous in riverine and coastal environments, but the physics governing morphodynamic interactions modulated by vegetation are still poorly understood. Here we use a simple experiment to study the impact of a vegetated patch on the morphodynamics of a sand bed. We show that the vegetation patch reduces the sediment transport capacity of the flow and that the topography responds to this by an increase of the bed slope to accommodate the upstream sediment supply. Final bed slope and adjustment time scale depend on the ratio between the grain-related shear stress and the total shear stress. This demonstrates the mechanisms underlying a direct morphodynamic response to the presence of a vegetation patch.

1. Introduction

Vegetation is a critical component of the morphodynamic and ecological evolution of coastal and riverine systems. Yet the physical processes by which it interacts with the flow and sediment beds are poorly understood. Vegetation is known to increase flow resistance, an effect that has traditionally been accounted for by an increased roughness coefficient in hydrodynamic models [*Fischenich*, 1997; *Ree and Palmer*, 1949; *Wilson*, 2007]. Recently, experimental investigations have provided an accurate description of how submerged vegetation affects velocity and turbulence profiles [*Fonseca et al.*, 1982; *Nepf and Vivoni*, 2000; *Carollo et al.*, 2002; *Stephan and Gutknecht*, 2002; *Poggi et al.*, 2004; *Järvelä*, 2005; *Lefebvre et al.*, 2010], and how turbulence is generated within canopies [*Raupach and Thom*, 1981; *Raupach et al.*, 1996] and at the interface between the vegetated and non-vegetated portions of the flow [*Nezu and Onitsuka*, 2001; *Ghisalberti and Nepf*, 2002].

The effect of such modifications of the flow on sediment transport has not been widely investigated. Observations in salt marshes suggest that vegetation increases deposition, a process by which the marsh can raise its surface [*Friedrichs and Perry*, 2001; *Bos et al.*, 2007; *Bouma et al.*, 2007] and persist with a rising sea level. This process has been shown to have a major influence on the long-term evolution of the marsh [*Temmerman et al.*, 2007; *Kirwan and Murray*, 2007; *D'Alpaos et al.*, 2007; *Marani et al.*, 2010]. Vegetation can also damp waves and reduce coastal erosion [*Turker et al.*, 2006]. In riverine environments, riparian vegetation has been shown to contribute to bank cohesion and exerts a major control on channel geometry [*Gran and Paola*, 2001; *Tal and Paola*, 2007; *Braudrick et al.*, 2009] and overbank deposition patterns [*Perignon et al.*, 2013], and thus has important implications for flood prevention and management. Vegetation and sediment transport also interact to create specific ecological habitats characterized by reduced flow velocity and wave energy [*Sanchez-Gonzalez et al.*, 2011; *Kobayashi et al.*, 1993], increased exchange rates of chemicals and nutrients due to vegetation-induced turbulence patterns, and a well-defined range of sediment grain size, geochemical composition, and turbidity values [*Madsen et al.*, 2001; *Sand-Jensen*, 1998; *Koch*, 2001]. Recent investigations also suggest that suspended sediment deposition patterns are governed by the changes in the velocity and turbulence fields induced by vegetation [*Zong and Nepf*, 2011; *Follett and Nepf*, 2012].

Despite recognition of the important role vegetation plays in flow dynamics and how those dynamics affect sediment transport, there has been little work focused on the direct morphodynamic evolution of sediment beds in response to vegetation [*Yager and Schmeeckle,* 2013]. Understanding this morphodynamic evolution is critical to sound coastal or river restoration projects that involve revegetation with the goal of restoring habitats [*Broome et al.*, 1988] and water quality [*Dosskey et al.*, 2010] or stabilizing the river channels. It is also important for flood management where vegetation alters stream and floodplain hydrodynamics and

Table 1. Flow and Sediment Transport Conditions at Equilibrium[a]

	Q	h	U	S_b	S_w	Q_{sb}	Q_{ss}	τ
	m^3/s	mm	m/s	%	%	g/s/m	g/s/m	Pa
Flow 1	0.05	136	0.37	0.77	0.26	1.96	2.71	3.78
Flow 2	0.04	142	0.28	0.63	0.21	0.35	0.31	3.23
Flow 3	0.035	153	0.23	0.15	0.11	0.14	0.13	1.58

[a] Q_{sb} and Q_{ss} are the bed load and suspended load transport rates.

responses to flood flows. Finally, as pointed out by *Nepf* [2012], ocean vegetation and especially seagrasses store carbon [*McLeod et al.*, 2011; *Fourqurean et al.*, 2012], and the morphodynamic evolution of sediment-plant systems impacts whether carbon is stored or released in response to changes in sea level and sediment supply to the ocean.

Here we present a series of experiments designed to investigate how sediment transport and morphodynamics respond to flexible submerged vegetation. We use a simple configuration of a water flow carrying sand through a vegetation patch. Vegetation in rivers and tidal environments is patchy by nature, and it is the distribution of patches and density of plants within those patches that controls the morphodynamic evolution of vegetated sedimentary environments. Our experiments demonstrate that the sediment transport capacity is reduced in the plants and that the bed adjusts by increasing its slope to pass the supply through the plant patch.

2. Methods

We performed experiments in a 12 m long, 1 m wide tilting flume that recirculates both water and sediment via two variable speed pumps. The central section of the flume between 5 and 11 m was covered with a simulated eelgrass bed. The eelgrass blades were made of a low-density (920 kg m^{-2}) polyethylene film (elastic modulus of 2×10^8 Pa), 25.5 cm long, 0.75 cm wide and 0.2 mm thick (see supporting information for photos). This material was chosen to ensure similarity between field and laboratory conditions for the ratio of the flexural rigidity and buoyancy [*Ghisalberti and Nepf*, 2002]. The plant density was 800 blades per square meter of bed, corresponding to a frontal area of 0.06 cm^{-1}, which is a characteristic value for the coastal eelgrass *Zostera marina* found on tidal flats in Southwestern Canada (C. Durance, Precision Identification, personal communication, 2011). Since the patch covers the full width of the flume, flow cannot divert laterally; therefore, the experiment is representative of wide meadow field conditions.

In addition to the plants, there was a sand bed of thickness ranging from 20 to 30 mm in the flume channel with a median grain size of the sand (D_{50}) of 150 μm and a narrow grain-size distribution (the 90th and 10th percentiles were 230 and 90 μm). The sand was transported as both bed load and suspended load. Three water discharges Q were used in the experiments (Table 1), corresponding to mean depth-averaged velocities U between 0.20 and 0.33 m s^{-1}, which are characteristic of flows on tidal flats where *Z. marina* are found (D. Ray, Northwest Hydraulic Consultants Ltd., personal communication, 2012). Water depth h was held constant in the experiments at approximately 150 mm. Flows were fully turbulent and subcritical in terms of the Froude number.

We monitored water surface elevation and topographic evolution of the sand bed during the experiments using a cart equipped with 32 echo-sounders and 3 ultrasonic water surface sensors. Bed load transport was monitored regularly by collecting and weighing sand at the flume outlet. Suspended sediment was measured using an L-shaped, 6.35 mm copper tube attached to an isokinetic pump, at three to four depths near the flume outlet and averaged over the full depth. Vertical velocity profiles were measured with an acoustic Doppler velocimeter at 50 Hz, approximately 3 m into the vegetation patch, on the centerline. At this location, the profiles are expected to be fully developed [see equation (10) in *Chen et al.*, 2013].

3. Observations

The water surface and bed slopes in the channel increased with discharge (Table 1) and were sub-parallel, which caused some convective acceleration through the eelgrass. So we calculated a total boundary

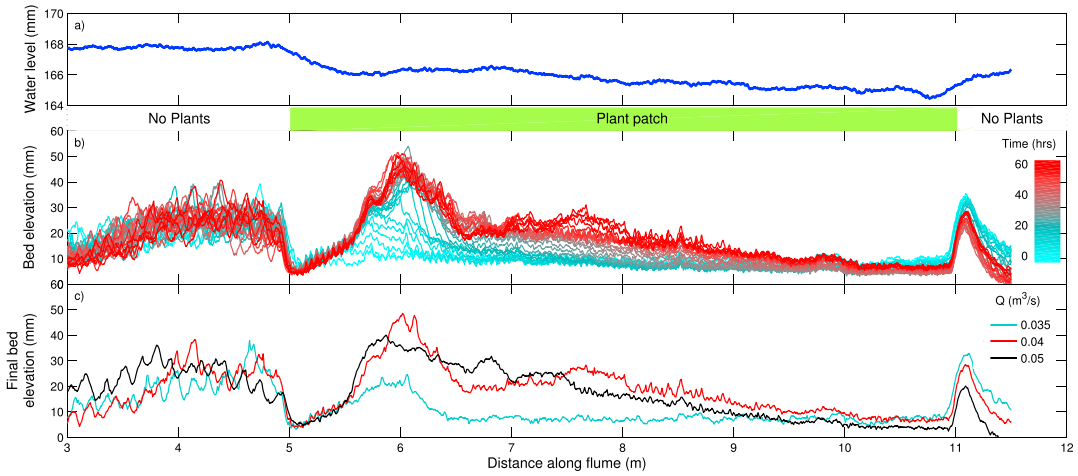

Figure 1. Profiles of (a) mean streamwise velocity $\bar{u}$, (b) turbulence intensity (u_{rms}), and (c) Reynolds shear stress for Flow 2, in the plant patch. Reynolds shear stress is calculated as $-\rho\overline{u'w'}$ where u' and w' are the fluctuations in the streamwise and vertical velocities relative to their means.

shear stress τ in the channel based on the 1-D shallow-water momentum equation (see derivation in the supporting information):

$$\tau = \rho g h S_w + \rho U^2 \frac{\partial h}{\partial x} \quad (1)$$

where ρ is the density of water, g is the gravitational acceleration, S_w is the water surface slope, U is the streamwise depth-averaged velocity, h is the water depth, and x is distance along the flume. Shear stress increased with discharge, even though the flow depth declined slightly (Table 1). Convective acceleration (the second term on the right in equation (1)) contributes between 2 and 18% to the shear stress (2, 10, and 18%).

Velocity and turbulence profiles obtained in the plants are plotted in Figure 1. The velocity profile shape is characteristic of a flow within a canopy, as observed in both field and laboratory experiments [*Nepf and Vivoni*, 2000; *Carollo et al.*, 2002; *Lacy and Wyllie-Echeverria,* 2011], for water as well as air flows [*Brunet et al.,* 1994]. The inflection point corresponds approximately to the location of the top of the canopy [*Nezu and Onitsuka*, 2001; *Nepf and Vivoni*, 2000] where a shear interface triggers Kelvin-Helmoltz instabilities. The growth of the Kelvin-Helmoltz vortices at the top of the canopy is reflected in the peak in the turbulence intensity (calculated as root mean square of fluctuating velocity: u_{rms}) and Reynolds shear stress profiles [*Nepf and Vivoni*, 2000; *Raupach et al.*, 1996]. A smaller peak in the turbulence and Reynolds stress profiles that is located close to the bottom reflects the influence of bed forms [*Nelson et al.,* 1993].

In each experiment, the sand bed evolved, adopting the same morphology. Figure 2b shows the evolution of the sand bed for Flow 2, which was characteristic of all the runs. Approaching the plant patch (3–5 m), the bed was relatively flat with ripples. A scour zone formed at the leading edge of the vegetation patch (5.0–5.5 m) eroding all the sand down to the flume bottom. Beyond the initial scour, a sand deposit formed that grew in elevation (5.5–6.5 m), progressively increasing the bed slope through the whole plant patch (6.5–11 m), ultimately reaching the equilibrium morphology shown in Figure 2b at 60 h. This morphodynamic adjustment occurred at all the flows tested (as shown in Figure 2c), although the adopted slope is dependent on the channel discharge (Table 1). At the exit of the eelgrass patch, another sand deposit formed (11–11.5 m).

4. Discussion

4.1. Reduction of the Sediment Transport Capacity

Comparison of measured bed load (Q_{sb}) and total load (Q_s) transport rates to predictions from several total load and bed load transport formulas, using the shear stress calculated in equation (1), indicates that the sediment transport is much lower than expected in the plant patch (Figure 3). However, τ incorporates all the possible sources of drag on the flow including: (1) the skin friction drag on the grain surfaces and form drag

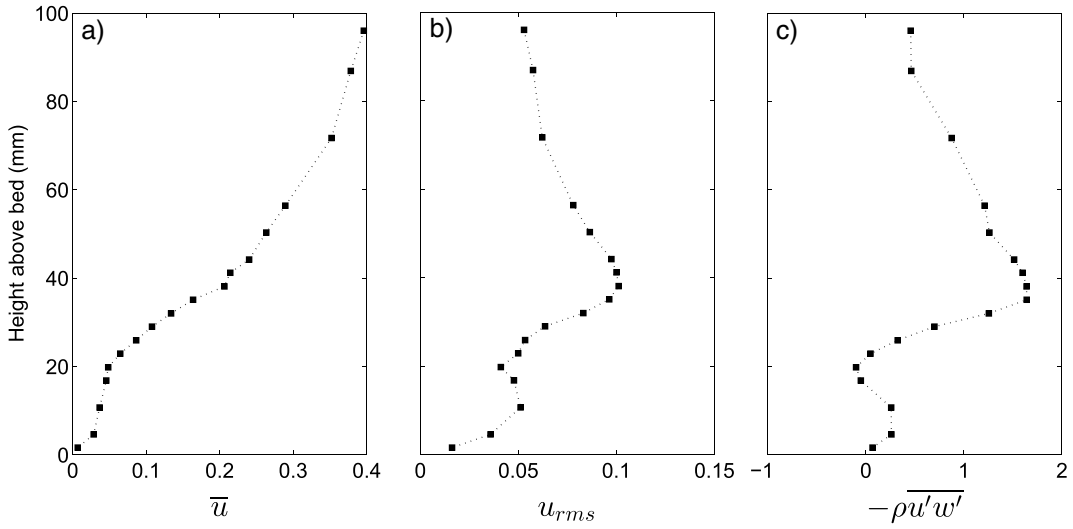

Figure 2. (a) Water level and (b) bed evolution from blue to red lines for Flow 2 over 60 h. Both elevations are measured with reference to the flume bottom. Note the change in scale between water and bed plots. (c) Final bed morphology for each of the three flows tested.

caused by pressure differentials about individual grains, the combination of which gives the grain-related shear stress τ_g responsible for sediment transport, (2) the form drag-related shear stress caused by accumulations of particles (bedforms) τ_b, and (3) the form drag-related shear stress borne by the plants τ_p. Reasonable sediment flux predictions require separation of these components [*Jordanova and James*, 2003]. The ratio of the grain-related shear stress to the total shear stress α can be calculated from

$$\alpha = \frac{\tau_g}{\tau} = \frac{\tau - \tau_b - \tau_p}{\tau}. \quad (2)$$

Calculation of τ_b and τ_p is not straightforward. We tested a variety of methods for partitioning shear stress and found that they all produced similarly small values of τ_g relative to τ. Inversion of bed load transport equations makes no assumptions about the flow and produces values of τ_g that increase with the bed load transport rate, which must inevitably be true (see supporting information). Values of α calculated from bed load transport equation inversion were nearly constant for all three flows ($\alpha = 8 \pm 2\%$ for Flow 1, $\alpha = 8 \pm 1\%$ for Flow 2, and $\alpha = 11 \pm 2\%$ for Flow 3; see supporting information for more details). As such, the vegetation and bed forms bear most of the total stress as form drag and should have a distinct effect on the sediment transport capacity in the plants.

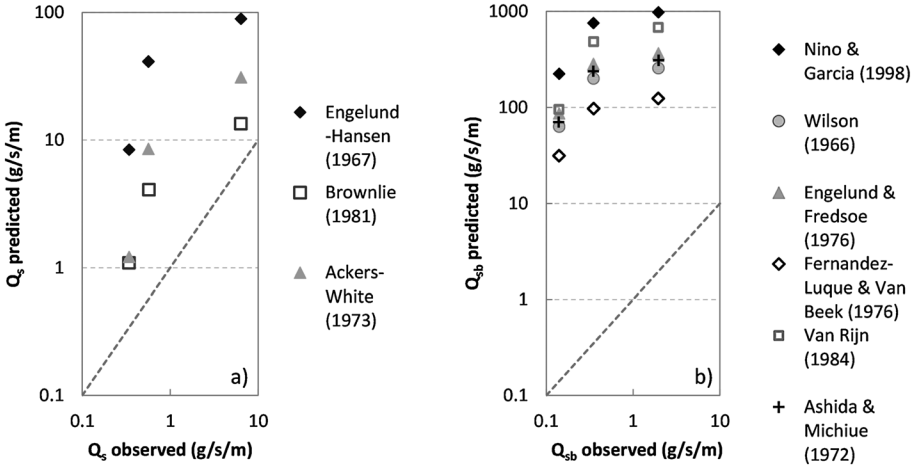

Figure 3. Predicted and observed values of (a) total sediment load (Q_s) and (b) bed load (Q_{sb}).

4.2. Local Scour and Deposition Patterns

The scour and deposition patterns that we observed on the vegetation edges are local features that result from the flow adjustment. Similar scour zones have been observed in the field measurements [e.g., *Bouma et al.*, 2007]. As the flow first encounters vegetation, it starts decelerating, but the velocity is still high enough to induce stem-generated turbulence, which has been shown to be associated with scour [*Follett and Nepf*, 2012]. Although turbulence levels have not been measured in this region, the length scale for the flow adjustment region can be estimated following *Chen et al.* [2013]:

$$L_0 \approx \frac{3}{C_p a}\left(1 + 2.3 C_p a h_p\right) \tag{3}$$

where a is the frontal area of the plants and C_p is the plant drag coefficient. Using $C_p = 1$ [*Nepf and Vivoni*, 2000] and with a deflected plant height $h_p \sim 45$ mm, equation (3) predicts an adjustment length scale of 0.83 m in our experiments, which is slightly higher than the observed length of the scour zone at the leading edge of the plants (Figure 2b). This suggests that the turbulence level drops as the velocity adjusts to a low value in the patch, limiting the spatial development of the scour. We observed that the length of the scour zone is roughly independent of the velocity magnitude. In their experiments, *Chen et al.* [2012] showed that L_o varies with the plant density (consistent with equation (3)).

While vegetation is commonly thought to produce a depositional environment, the scour zone indicates that it also has the ability to locally erode the topography [*Bouma et al.*, 2007; *Temmerman et al.*, 2007]. This suggests that the spatial arrangement and physical scale of plant patches play an important role in the morphodynamic response. Plant patches smaller than L_o are likely to induce erosion and be unstable. Conversely, patches longer than L_o are likely to induce deposition within and behind the patch, creating conditions favorable to colonization/expansion of the vegetation and colonization in the downstream direction [*Sand-Jensen and Madsen*, 1992].

4.3. Morphodynamic Adjustment to Vegetated Patch

The evolution of the bed is a morphodynamic adjustment from a spatially (in the downstream direction) non-uniform sediment transport field to a uniform transport field with equilibrium topography. The flume is not covered with plants along its entire length, so flow (water surface slope, velocity profiles), topography, and the sediment transport rate adjust to the presence of the patch. Flow enters the vegetation patch with a sediment load that corresponds to upstream transport capacity. After the scour zone, sediment starts depositing in the plant patch, because the plants carry a portion of the total stress, reducing the stress exerted on the sediment grains. In order to reach steady-state topography, the sediment transport rate must be uniform in the alongstream direction. So the transport capacity through the plants must be increased to pass the load coming from the unvegetated part of the flume. This is accomplished by an increase in the water surface and bed slopes to increase the total shear stress, and in so doing the grain-related shear stress in the patch. A similar topographic adjustment was observed in the field by *Fonseca et al.* [1983]. We can demonstrate that the evolution of the bed morphology is the result of the non-uniformity of the sediment flux using the Exner equation:

$$\rho_s(1-\varphi)\frac{\partial \eta}{\partial t} = -\frac{\partial q_s}{\partial x} \tag{4}$$

where φ is the porosity of the bed, ρ_s is the sediment density, and η is the bed elevation, x is distance along the flume, t is time, and q_s is the local sediment flux in the plant patch. Using a series of bed scans taken every 40 min over 60 h, q_s is computed by integrating equation (7) along the streamwise direction (referred to as x' inside the integral):

$$q_s(x,t) = q_s(x_0,t) + \int_{x_0}^{x} -\rho_s(1-\varphi)\frac{\partial \eta}{\partial t}(x',t)dx' \tag{5}$$

Using the leading edge of the plant patch x_0 as a reference for the integration, the change in sediment flux from the reference point or relative sediment flux, $q_s(x, t) - q_s(x_0, t)$ is plotted in Figure 4. Equilibrium sediment flux is reached when $q_s(x, t) - q_s(x_0, t) = 0$ along the whole flume.

At the beginning of the run, the sediment flux was lower throughout the plants than at the entrance of the patch; $q_s(x) < q_s(x_0)$. Then, as the bed built up in the plant patch, the sediment flux in the plants progressively

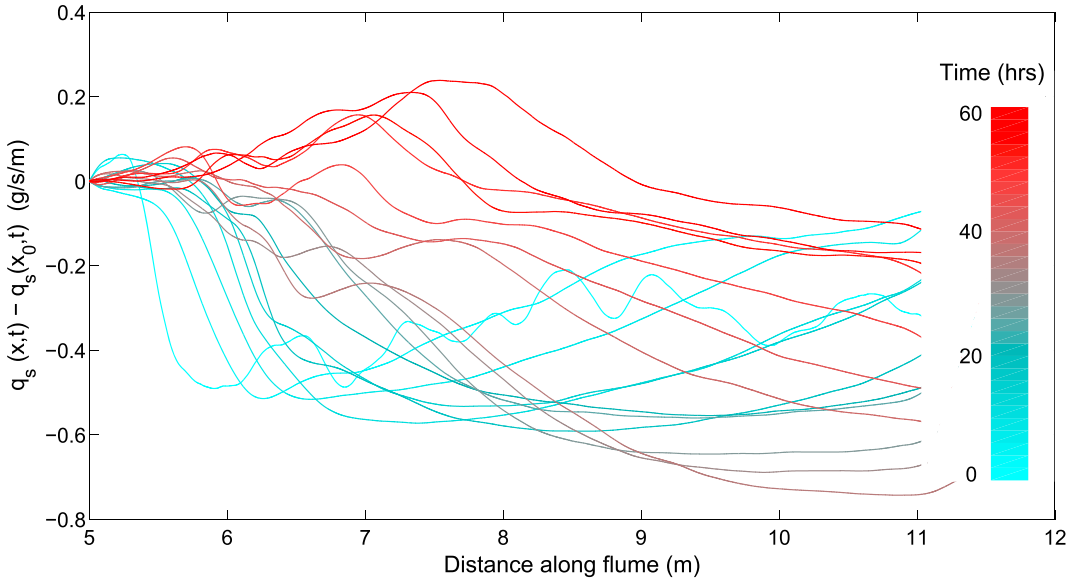

Figure 4. Evolution of the sediment flux $q_s(x, t)$ in the plant patch relative to its value at the entrance of the patch $q_s(x_0, t)$ over 60 h. The relative sediment flux is calculated using equation (8) with $x_0 = 5$ m (the entrance of the plant patch), plotted every 200 min, starting at $t = 0$ h.

adjusted to equal this imposed value (Figure 4). Equilibrium sediment flux was reached at the most upstream locations first and then propagated through the plant patch. We observed a cyclic process whereby sediment was temporarily stored at 7–9 m, then released as a pulse. This caused some variability in the equilibrium bed morphology and gave rise to migrating peaks in relative sediment flux in the later stage of the experiment. The system reaches equilibrium when the bed slope in the plants is high enough for the sediment transport capacity in the patch to be equal to that of the non-vegetated upstream section.

The bed slope increase is therefore a response to a non-uniform sediment transport field. Given that α is nearly constant for a given density of plants, maintaining a constant sediment flux q_s requires increasing the shear stress (τ). Although the bed slope S_b and water surface slope S_w do not match in our experiments, they are positively correlated. So the increase in τ needed to maintain Q_s is achieved by increasing S_b and S_w, as observed in the experiments. The ratio α is therefore the critical parameter that governs the morphodynamic response. More research is needed to investigate how α varies with other factors, including the plant density.

4.4. Time Scale of Morphodynamic Adjustment

Sediment deposition in the plants is a transitory response. Once the slope has increased enough for the flow to transport the incoming sediment flux, equilibrium is reached and no more deposition is expected. This has some important implications for river restoration and soil conservation methods. It is often argued that adding/restoring vegetation in channels creates a sediment sink that reduces the sediment yield from the catchment [*Rey,* 2004; *Molina et al.*, 2009]. Our results suggest that this reduction is a transitory effect until the slope has increased enough to accommodate the incoming sediment load.

If the bed slope without plants is S_{np}, and assuming that the bed slope matches the water surface slope on the long term, maintaining a constant sediment flux Q_s when plants are present requires that the grain-related shear stresses with and without the plants are the same. If we assume that $\tau = f(\rho g h S)$, that h does not change significantly when the plants are present and that we can neglect the form drag component of the bed forms, which is relatively small compared to that of the plants (Figure 1) the equilibrium slope with plants is $S_e = S_{np}/\alpha$. The time scale t_e of the response scales with the skin friction coefficient α

$$t_e \sim L^2 S_{np} \rho_s (1-\varphi)(1-\alpha)/(2Q_s\alpha) \quad (6)$$

where L is the patch length (see derivation in the supporting information). Equation (6) yields values of 7, 75, and 184 h for flows 1, 2, and 3 in our experiments, which are realistic compared to our observations. This

would also suggest that Flow 3 has not reached equilibrium conditions at the end of the experiment and that further deposition may be expected. Note that our experiments do not take into account subsidence, nor the growth of the vegetation. One can expect that if the vegetation grows not only in height but also in density (side branches, leaves), this could increase the value of α, therefore the time needed for equilibrium. A subsiding environment would also allow sediment retention on a longer term.

5. Conclusions

Introduction of flexible vegetation to a sediment bed alters the balance of fluid forces. The portion of the total fluid shear stress exerted on plants reduces the grain-related shear stress applied to the bed. The morphodynamic response is to increase the local slope to pass the incoming sediment load to maintain sediment continuity. The rate at which the bed evolves to equilibrium varies with the magnitude of the flow. However, the proportion of the total shear stress exerted on the sediment grains is nearly invariant with flow, so the morphologic adjustment is always the same for a given density of plants. As such, understanding the ratio of the grain-related to total bed shear stress is critical to predicting the morphodynamic response of sediment beds to vegetation and its time scale.

Acknowledgments

The data that were used for this paper can be made available upon request from the authors. The project was funded by a fellowship from Mitacs Canada and Northwest Hydraulic Consultants Ltd. We thank Dave McLean and Derek Ray for their encouragement to work on the problem. We also thank Jacqui Brown and Malcolm Little for their help in the laboratory.

The Editor thanks Chris Paola and an anonymous reviewer for their assistance in evaluating this manuscript.

References

Bos, A. R., T. J. Bouma, G. L. De Kort, and M. M. Van Katwijk (2007), Ecosystem engineering by annual intertidal seagrass beds: Sediment accretion and modification, *Estuarine Coastal Shelf Sci.*, *74*, 344–348, doi:10.1016/j.ecss.2007.04.006.

Bouma, T. J., L. A. Van Duren, S. Temmerman, T. Claverie, A. Blanco-Garcia, T. Ysebaert, and P. M. J. Herman (2007), Spatial flow and sedimentation patterns within patches of epibenthic structures: Combining field, flume and modelling experiments, *Cont. Shelf Res.*, *27*, 1020–1045, doi:10.1016/j.csr.2005.12.019.

Braudrick, C., W. Dietrich, G. C. Leverich, and L. Sklar (2009), Experimental evidence for the conditions necessary to sustain meandering in coarse-bedded rivers, *Proc. Natl. Acad. Sci. U. S. A.*, *106*, 16,936–16,941, doi:10.1073/pnas.0909417106.

Broome, S., E. Seneca, and W. Woodhouse Jr. (1988), Tidal salt marsh restoration, *Aquat. Bot.*, *32*, 1–22.

Brunet, Y., J. Finnigan, and M. Raupach (1994), A wind-tunnel study of air-flow in waving wheat - single point velocity statistics, *Boundary Layer Meteorol.*, *70*, 95–132.

Carollo, F., V. Ferro, and D. Termini (2002), Flow velocity measurements in vegetated channels, *J. Hydraul. Eng. ASCE*, *128*, 664–673.

Chen, S., H. Chan, and Y. Li (2012), Observations on flow and local scour around submerged flexible vegetation, *Adv. Water Resour.*, *43*, 28–37.

Chen, Z., C. Jiang, and H. Nepf (2013), Flow adjustment at the leading edge of a submerged aquatic canopy, *Water Resour. Res.*, *49*, 5537–5551, doi:10.1002/wrcr.20403.

D'Alpaos, A., S. Lanzoni, M. Marani, and A. Rinaldo (2007), Landscape evolution in tidal embayments: Modeling the interplay of erosion, sedimentation, and vegetation dynamics, *J. Geophys. Res.*, *112*, F01008, doi:10.1029/2006JF000537.

Dosskey, M., P. Vidon, N. D. Gurwick, C. Allan, T. Duval, and R. Lowrance (2010), The role of riparian vegetation in protecting and improving chemical water quality in streams, *J. Am. Water Resour. Assoc.*, *46*, 261–277, doi:10.1111/j.1752-1688.2010.00419.x.

Fischenich, J. (1997), Hydraulic impacts of riparian vegetation; summary of the literature, *U.S. Army Corps of Engineers Technical Report EL-97-9.*

Follett, E., and H. Nepf (2012), Sediment patterns near a model patch of reedy emergent vegetation, *Geomorphology*, *179*, 141–151, doi:10.1016/j.geomorph.2012.08.006.

Fonseca, M., J. Fisher, J. Zieman, and G. Thayer (1982), Influence of the seagrass, zostera marina l., on current flow, *Estuarine Coastal Shelf Sci.*, *15*, 351–364.

Fonseca, M. S., J. C. Zieman, G. W. Thayer, and J. S. Fisher (1983), The role of current velocity in structuring seagrass meadows, *Estuarine Coastal Shelf Sci.*, *17*, 367–380.

Fourqurean, J., et al. (2012), Seagrass ecosystems as a globally significant carbon stock, *Nat. Geosci.*, *5*, 505–509, doi:10.1038/ngeo1477.

Friedrichs, C. T., and J. E. Perry (2001), Tidal salt marsh morphodynamics: A synthesis, *J. Coastal Res.*, *special issue 27*, 7–37.

Ghisalberti, M., and H. Nepf (2002), Mixing layers and coherent structures in vegetated aquatic flows, *J. Geophys. Res. 107*(C2), 3011, doi:10.1029/2001JC000871.

Gran, K., and C. Paola (2001), Riparian vegetation controls on braided stream dynamics, *Water Resour. Res.*, *37*, 3275–3283, doi:10.1029/2000WR000203.

Järvelä, J. (2005), Effect of submerged flexible vegetation on flow structure and resistance, *J. Hydrol.*, *307*, 233–241, doi:10.1016/j.jhydrol.2004.10.013.

Jordanova, A. A., and C. S. James (2003), Experimental study of bedload transport through emergent vegetation, *J. Hydraul. Eng.*, *129*(6), 474–478, doi:10.1061/(ASCE)0733-9429(2003)129:6(474.

Kirwan, M. L., and A. B. Murray (2007), A coupled geomorphic and ecological model of tidal marsh evolution, *Proc. Natl. Acad. Sci. U. S. A.*, *104*, 6118–6122, doi:10.1073/pnas.0700958104.

Kobayashi, N., A. Raichle, and T. Asano (1993), Wave attenuation by vegetation, *J. Waterway Port Coastal Ocean Eng. ASCE*, *119*, 30–48.

Koch, E. (2001), Beyond light: Physical, geological, and geochemical parameters as possible submersed aquatic vegetation habitat requirements, *Estuaries*, *24*, 1–17.

Lacy, J. R., and S. Wyllie-Echeverria (2011), The influence of current speed and vegetation density on flow structure in two macrotidal eelgrass canopies, *Limnol. Oceanogr. Fluids Environ.*, *1*, 38–55, doi:10.1215/21573698-1152489.

Lefebvre, A., C. E. L. Thompson, and C. L. Amos (2010), Influence of Zostera Marina canopies on unidirectional flow, hydraulic roughness and sediment movement, *Cont. Shelf Res.*, *30*, 1783–1794, doi:10.1016/j.csr.2010.08.006.

Madsen, J. B., P. Chambers, W. James, E. Koch, and D. Westlake (2001), The interaction between water movement, sediment dynamics and submersed macrophytes, *Hydrobiologia*, *444*, 71–84, doi:10.1023/A:1017520800568.

Marani, M. B., A. D'Alpaos, S. Lanzoni, L. Carniello, and A. D. Rinaldo (2010), The importance of being coupled: Stable states and catastrophic shifts in tidal biomorphodynamics, *J. Geophys. Res.*, *115*, F04004, doi:10.1029/2009JF001600.

McLeod, E., G. Chmura, S. Bouillon, R. Salm, M. Bjork, C. F. Duarte, C. Lovelock, W. Schlesinger, and B. Silliman (2011), A blueprint for blue carbon: Toward an improved understanding of the role of vegetated coastal habitats in sequestering CO_2, *Front. Ecol. Environ.*, *9*, 552–560, doi:10.1890/110004.

Molina, A., G. Govers, F. Cisneros, and V. Vanacker (2009), Vegetation and topographic controls on sediment deposition and storage on gully beds in a degraded mountain area, *Earth Surf. Proc. Land.*, *34*, 755–767, doi:10.1002/esp.1747.

Nelson, J., S. McLean, and S. Wolfe (1993), Mean flow and turbulence fields over two-dimensional bed forms, *Water Resour. Res.*, *29*, 3935–3953, doi:10.1029/93WR01932.

Nepf, H. (2012), Hydrodynamics of vegetated channels, *J. Hydraul. Res.*, *50*, 262–279, doi:10.1080/00221686.2012.696559.

Nepf, H., and E. Vivoni (2000), Flow structure in depth-limited, vegetated flow, *J. Geophys. Res.*, *105*, 28,547–28,557, doi:10.1029/2000JC900145.

Nezu, I., and K. Onitsuka (2001), Turbulent structures in partly vegetated open-channel flows with lda and piv measurements, *J. Hydraul. Res.*, *39*, 629–642.

Perignon, M. C., G. E. Tucker, E. R. Griffin, and J. M. Friedman (2013), Effects of riparian vegetation on topographic change during a large flood event, Rio Puerco, New Mexico, USA, *J. Geophys. Res. Earth Surf.*, *118*, 1193–1209, doi:10.1002/jgrf.20073.

Poggi, D., A. Porporato, L. Ridolfi, J. Albertson, and G. Katul (2004), The effect of vegetation density on canopy sublayer turbulence, *Boundary Layer Meteorol.*, *111*, 565–587, doi:10.1023/B:BOUN.0000016576.05621.73.

Raupach, M., and A. S. Thom (1981), Turbulence in and above plant canopies, *Annu. Rev. Fluid Mech.*, *13*, 97–129.

Raupach, M., J. Finnigan, and Y. Brunet (1996), Coherent eddies and turbulence in vegetation canopies: The mixing-layer analogy, *Boundary Layer Meteorol.*, *78*, 351–382.

Ree, W. and V. Palmer (1949), Flow of water in channels protected by vegetative linings, *U.S. Department of Agriculture, Soil Conservation Service Technical Bulletin 967*.

Rey, F. (2004), Effectiveness of vegetation barriers for marly sediment trapping, *Earth Surf. Proc. Land.*, *29*, 1161–1169, doi:10.1002/esp.1108.

Sanchez-Gonzalez, J., V. Sanchez-Rojas, and C. Memos (2011), Wave attenuation due to Posidonia Oceanica meadows, *J. Hydraul. Res.*, *49*, 503–514, doi:10.1080/00221686.2011.552464.

Sand-Jensen, K. (1998), Influence of submerged macrophytes on sediment composition and near-bed flow in lowland streams, *Freshwater Biol.*, *39*, 663–679.

Sand-Jensen, K., and T. Madsen (1992), Patch dynamics of the stream macrophyte, callitriche cophocarpa, *Freshwater Biol.*, *27*, 277–282, doi:10.1046/j.1365-2427.1998.00316.x.

Stephan, U., and D. Gutknecht (2002), Hydraulic resistance of submerged flexible vegetation, *J. Hydrol.*, *269*, 27–43, doi:10.1016/S0022-1694(02)00192-0.

Tal, M., and C. Paola (2007), Dynamic single-thread channels maintained by the interaction of flow and vegetation, *Geology*, *35*, 347–350, doi:10.1130/G23260A.1.

Temmerman, S., T. J. Bouma, J. Van de Koppel, D. Van der Wal, M. B. De Vries, and P. M. J. Herman (2007), Vegetation causes channel erosion in a tidal landscape, *Geology*, *35*, 631–634, doi:10.1130/G23502A.1.

Turker, U., O. Yagci, and M. Kabdasli (2006), Analysis of coastal damage of a beach profile under the protection of emergent vegetation, *Ocean Eng.*, *33*(5-6), 810–828, doi:10.1016/j.oceaneng.2005.04.019.

Wilson, C. A. (2007), Flow resistance models for flexible submerged vegetation, *J. Hydrol.*, *342*, 213–222, doi:10.1016/j.jhydrol.2007.04.022.

Yager, E. M., and M. W. Schmeeckle (2013), The influence of vegetation on turbulence and bed load transport, *J. Geophys. Res. Earth Surf.*, *118*, 1585–1601, doi:10.1002/jgrf.20085.

Zong, L., and H. Nepf (2011), Spatial distribution of deposition within a patch of vegetation, *Water Resour. Res.*, *47*, W03516, doi:10.1029/2010WR009516.

Auxiliary Material for

Morphodynamic adjustment of a sand bed to a patch of vegetation.

Caroline Le Bouteiller (1, 2) and Jeremy G. Venditti (1)

1 Department of Geography, Simon Fraser University, Burnaby, British Columbia, V5A 1S6, Canada

2 Now at: IRSTEA, UR ETNA, F-38402 Saint-Martin d'Heres, France

Geophysical Research Letters

Introduction

This additional information contains both photographs of the experiments described in the paper, detailed mathematical derivations for two equations used in the paper and detailed results from the bedload transport formula inversion used in the paper. Photos were taken during summer 2012 in the Environmental Fluid and Sediment Dynamics Laboratory at Simon Fraser University, Burnaby, Canada.

1. fs01.eps : photographs of the experiment. Flow is from right to left

2. text01.doc : detailed derivation of Equation 1

3. text02.doc: results from bedload formula inversion

4. text03.doc : detailed derivation of Equation 6

Auxiliary Material: Derivation of Equation 1 from the Saint-Venant shallow water equations

Depth-integrated equations for flow momentum and mass balance in a one-dimensional framework are:

$$\frac{\partial U}{\partial t} + U\frac{\partial U}{\partial x} = -g\frac{\partial h}{\partial x} + gS_b - \frac{\tau}{\rho h} \qquad \text{(Equation S1a)}$$

$$\frac{\partial h}{\partial t} + U\frac{\partial h}{\partial x} = -h\frac{\partial U}{\partial x} \qquad \text{(Equation S1b)}$$

Where U is mean flow velocity, h is mean flow depth, g is gravity, S_b is the bed slope (with a positive value when sloping in the downstream direction) and τ is the bottom shear stress. Assuming a permanent flow, time-derivative are equal to zero. Calling z_b the bottom elevation and z_w the elevation of the water surface, one can write that:

$$S_b - \frac{\partial h}{\partial x} = -\left(\frac{\partial z_b}{\partial x} + \frac{\partial h}{\partial x}\right) = -\frac{\partial z_w}{\partial x} = S_w \qquad \text{(Equation S2)}$$

Where S_w is the water surface slope. Equation S1a then reduces to:

$$U\frac{\partial U}{\partial x} = gS_w - \frac{\tau}{\rho h} \qquad \text{(Equation S3)}$$

Using Equation S1b in its permanent form, it is finally possible to transform Equation S3 into the simple following form:

$$\tau = \rho g h S_w + \rho U^2\frac{\partial h}{\partial x} \qquad \text{(Equation S4)}$$

First term on the right side of Equation S4 is the common depth-slope product used to calculate the bottom shear stress in uniform flow conditions while the second-term results from the convective acceleration generated as the flow section changes.

Finally, the water depth in the first term of the right-hand side of Equation S4 is corrected according to the Vanoni and Brooks' method in order to account for the friction generated by the side walls. As the side walls are much smoother than the vegetated bed, this correction only represents a 2 to 4% change in the computed shear stress.

Auxiliary material: Calculation of the grain-related shear stress by inverting bedload formulas

Bedload transport is usually assumed to be induced by the grain-related shear stress (skin friction at the grain surfaces and form drag around individual grains). Bedload formulas predict bedload transport rate based on the grain-related shear stress. In order to calculate this grain-related shear stress τ_g, we use the measurements of bedload transport rates (see Table 1) and invert bedload formulas.

While bedload formulas are known to produce reasonable estimates of transport rates in simple experimental configurations, they can be more problematic in complex channels, so rather than relying on a single bedload transport equation, we calculate the grain-related shear stress using 6 bedload equations and use an ensemble average of the results for inversion. Results of the calculation are presented in Table S1 and show that the equations all produce similar values.

Table S1: Grain-related shear stress obtained by inverting several bedload formulas.

	Nino & Garcia (1998)	Ashida & Michiue (1972)	Wilson (1966)	Engelund & Froedse (1976)	Fernandez -Luque & Van Beek (1976)	Van Rijn (1984)			
	τ_g (Pa)	τ_g (Pa)	τ_g (Pa)	τ_g (Pa)	τ_g (Pa)	τ_g (Pa)	Avg. τ_g (Pa)	Std τ_g (Pa)	Std/Avg (%)
Flow 1	0.23	0.3	0.3	0.25	0.35	0.39	0.3	0.06	20
Flow 2	0.18	0.19	0.21	0.16	0.19	0.26	0.2	0.03	15
Flow 3	0.17	0.17	0.19	0.14	0.16	0.23	0.17	0.03	18

Based on the average values of τ_g, the α ratio is then estimated following equation (2), which yields $\alpha = 8 \pm 2\%$ for Flow 1, $\alpha = 8 \pm 1\%$ for Flow 2 and $\alpha = 11 \pm 2\%$ for Flow 3 (the error range is the standard deviation of the predictions).

Le Bouteiller and Venditti (in preparation) also tested a variety of other methods for partitioning shear stress including 1) Einstein and Banks (1950), 2) Smith and McLean (1977), modified to account for plant drag, 3) near-bed Reynolds stress, and 4) Shao and Yang (2008), and all produced similarly small values of τ_g relative to τ, so the values produced by inversion of bedload transport equations are a reasonable approximation of τ_g. Inversion of bedload transport equations also carries the fewest assumptions about the flow. Furthermore, the bedload transport equation inversion suggests that the plant density is a primary control on α, which is consistent with Chen et al. (2012) and produces values of τ_g that increase with the bedload transport rate, which must inevitably be true.

Einstein, H.A., and Banks, R.B. (1950), Fluid resistance of composite roughness. *Transactions, American Geophysical Union 31*

Smith, J. D., and S. R. McLean (1977), Spatially averaged flow over a wavy surface, *J. Geophys. Res. 82(12)*, 1735–1746

Shao, Y., and Y. Yang (2008), A theory for drag partition over rough surfaces, *J. Geophys. Res. 113*, F02S05, doi:10.1029/2007JF000791

Auxiliary Material: Derivation of Equation 6 for Equilibrium Time Scale for Morphodynamics Adjustment

(Variables not defined below are defined in the main text)

The sediment flux without the plants is

$$Q_s = f(\tau)$$

where the total shear stress is calculated as

$$\tau = \rho g H S_{np}.$$

The skin-related shear stress responsible for driving sediment transport is presumed to be proportional to τ for any given condition (plants or no plants). If we neglect the form drag component of the bedforms, which is relatively small compared to that of the plants (Le Bouteiller and Venditti, in review), the sediment flux with the plants is

$$Q_{se} = f(\alpha\tau_e)$$

and

$$\tau_e = \rho g H_e S_e$$

where the subscript e indicates equilibrium conditions with the plants. In order to pass the imposed sediment flux, $Q_s = Q_{se}$. Therefore

$$\tau = \alpha\tau_e$$

and

$$\rho g H S_{np} = \alpha\rho g H_e S_e.$$

If we assume that $H \approx H_e$ the adjustment in slope required for $Q_s = Q_{se}$ is $S_e = S_{np}/\alpha$. This assumption is consistent with our experiments, in so far as the adjustment in shear stress from a condition with no plants to one with plants occurs by adjusting the slope, not depth.

The time scale for adjustment from a bed with no plants to one with plants is based on the geometry of the deposit required to build the slope from S to S_e. The per unit width volume of sediment needed to fill the space between slope S and slope S_e is given by

$$V = S_e L^2/2 - S_{np} L^2/2 = L^2 S_{np} (1/\alpha\text{-}1)/2$$

The sediment mass needed to increase the slope is

$$M = V \rho_s (1 - \varphi).$$

Sediment is supplied at rate Q_s, so the time needed to increase the slope (assuming all the supplied sediment is stored in the bed while the slope has not reached equilibrium) is

$$t_e = M / Q_s = V \rho_s (1 - \varphi) / Q_s = L^2 S_{np} (1/\alpha - 1) \rho_s (1 - \varphi) / 2Q_s.$$